

Supporting Information

Selective Organic Transformation Over Self-Assembled All-Solid-State Z-scheme Core-Shell Photoredox System

Xin Lin, Shuai Xu, Zhi-Quan Wei, Shuo Hou, Qiao-Ling Mo, Xiao-Yan Fu, Fang-Xing Xiao*

College of Materials Science and Engineering, Fuzhou University, New Campus, Minhou, Fujian

Province 350108, China.

E-mail: fx Xiao@fzu.edu.cn

Experimental details

1. Materials

Sodium tungstate dihydrate ($\text{Na}_2\text{WO}_4\cdot\text{H}_2\text{O}$), Sodium chloride (NaCl), Hydrochloric acid (HCl), Sodium tetrachloropalladate (Na_2PdCl_4), Tetraoctyl ammonium bromide (TOAB), Toluene, sodium borohydride (NaBH_4), Sodium sulfate anhydrous (Na_2SO_4), Sodium hydroxide (NaOH), Sulfuric acid (H_2SO_4), 4-dimethylaminopyridine (DMAP), Potassium peroxydisulfate ($\text{K}_2\text{S}_2\text{O}_8$), Sodium sulfite (Na_2SO_3), Ammonium oxalate (AO), *p*-Benzoquinone ($\text{C}_6\text{H}_4\text{O}_2$), Tert-butanol ($\text{C}_4\text{H}_{10}\text{O}$), Cadmium chloride ($\text{CdCl}_2\cdot 2.5\text{H}_2\text{O}$), Sublimed Sulfur (S), *p*-Phthalic acid (PTA) and Deionized water (DI H_2O , Millipore, $18.2\text{ M}\Omega\cdot\text{cm}$ resistivity), were obtained from Sinopharm Chemical Reagent Co., Ltd. (Shanghai China). Ammonium formate (HCOONH_4), 4-nitroaniline (4-NA), 3-nitroaniline (3-NA), 2-nitroaniline (2-NA), 4-nitrophenol (4-NP), 3-nitrophenol (3-NP), 2-nitrophenol (2-NP), 4-nitrotoluene (4-NT), 4-nitroanisole, nitrobenzene, *o*-nitroacetophenone, 1-chloro-4-nitrobenzene and 1-bromo-4-nitrobenzene were obtained from Aladdin Industrial Corporation (Shanghai, China). Benzotrifluoride (BTF), Benzyl alcohol (BA), *p*-methylbenzyl alcohol (*p*-MBA), *p*-methoxybenzyl alcohol (*p*-MOBA), *p*-fluorobenzyl alcohol (*p*-FBA), *p*-chlorobenzyl alcohol (*p*-CBA), *p*-nitrobenzyl alcohol (*p*-NBA), Cinnamyl alcohol (CA), and 3-methyl-2-buten-1-ol (3A) were obtained from Alfa Aesar (China) Chemicals Co., Ltd. All the materials were used as received without further treatment.

2. Preparation of WO_3 nanorods (NRs)

WO_3 NRs were synthesized by a one-step hydrothermal treatment.^{S1} Specifically, 1.056 g of $\text{Na}_2\text{WO}_4\cdot 2\text{H}_2\text{O}$ and 0.935 g of NaCl were dissolved in 30 mL of DI H_2O and kept stirring for 20 min. The pH value of the mixed solution was adjusted to ca. 2 using HCl (3.0 M) aqueous solution, and then the solution was vigorously stirred for 2 h. After that, the solution was transferred to a Teflon-lined autoclave (100 mL) and maintained at $180\text{ }^\circ\text{C}$ for 24 h. Afterwards, the products were

cooled to room temperature, separated by centrifugation, and washed with DI H₂O. Eventually, the sediment was dried at 60 °C.

3. Preparation of Pd@DMAP nanocrystal

Preparation of Pd@DMAP was referred to a published work.^{S2} Prior to experiment, all glassware were cleaned thoroughly with aqua (3:1 in volume for HCl and HNO₃) for 12 h and thoroughly washed with DI H₂O. A 30 mM aqueous Na₂PdCl₄ solution (30 mL) was added to a 25 mM TOAB solution in toluene (80 mL). The transfer of the gold salt to the toluene phase can be seen within a few seconds. A freshly prepared 0.4 M NaBH₄ (25 mL) aqueous solution was added to the above mixture under vigorous stirring. After 30 min, the two phases were separated and the toluene phase was subsequently washed with 0.1 M H₂SO₄, 0.1 M NaOH, and DI H₂O for three times, and then dried with anhydrous Na₂SO₄. Afterwards, an aqueous 0.1 M 4-dimethylaminopyridine (DMAP) solution (80 mL) was added into aliquots (80 mL) of the as-prepared nanoparticle mixtures. Direct phase transfer across the organic/aqueous interface was completed within 2 h with no stirring or agitation required. Finally, Pd-dissolved water phase was separated by a separatory funnel and Pd@DMAP aqueous solution was thus obtained.

4. Self-assembly of WO₃ NRs@Pd heterostructures

WO₃ NRs@Pd heterostructures with different weight percentage of Pd were fabricated by an electrostatic self-assembly method at ambient conditions. Specifically, intrinsically positively charged Pd@DMAP aqueous solution (1.2 mgmL⁻¹) was diluted to 0.1 mgmL⁻¹, after which different amount of Pd@DMAP aqueous suspension (0.1 mgmL⁻¹, pH=10) was added dropwise to the negatively charged WO₃ NRs aqueous dispersion (2 mgmL⁻¹, pH=10) under vigorous stirring for 2h at ambient conditions. The weight percentage of Pd@DMAP in the nanocomposites was controlled to be 1, 3, 5, 7, 9 and 11% by adding the corresponding volumes of 10, 30, 50, 70, 90 and

110 mL into the WO₃ NRs aqueous solution, respectively. Finally, the mixture was centrifuged and dried in an oven at 333 K.

5. Preparation of WO₃ NRs@Pd@CdS core-shell heterostructure

As stated in the Manuscript, in a typical procedure, 40 mg of CdCl₂·2.5H₂O and 10 mg of S₈ were dispersed in 50 mL of ethanol to form a stable suspension and bubbled with N₂ for 30 min in the dark.^{S3} The WO₃ NRs@Pd nanocomposite was immersed in the above suspension and irradiated for different times under simulated solar light (300 W Xe arc lamp, PLS-SXE300D, Beijing Perfectlight Co. Ltd, China). The samples were rinsed with ethanol/DI H₂O and dried in a vacuum oven at 60 °C.

6. Photocatalytic oxidation of organic pollutant

10 mg of catalyst was dispersed in 40 mL of Rh B aqueous solution (5 ppm). The reaction system was firstly stirred in the dark for 0.5 h and then irradiated with (300 W Xe lamp, PLS-SXE300D, Beijing Perfectlight Co. Ltd, China) visible light ($\lambda > 420$ nm). 3 mL of the solution was withdrawn at every 30 min interval, centrifuged, and analyzed by UV-vis absorption spectrophotometer (Genesys 10S, Thermo Scientific).

7. Determination of the active species

(a) Detection of active species by quenching experiments.

Quenching experiments were conducted under the same experimental conditions as that of the photodegradation reactions except for adding 1.0 mM scavengers in the reaction system. Different scavengers such as benzoquinone (BQ), tert-butyl alcohol (TBA), ammonium oxalate (AO) and K₂S₂O₈ were utilized as the scavengers for quenching superoxide radicals ($\bullet\text{O}^{2-}$), hydroxyl radicals ($\bullet\text{OH}$), holes (h^+) and electrons (e^-), respectively.

(b) Determination of $\bullet\text{OH}$ radicals^{S4, S5}

The experimental procedure was similar to the photoactivity test for dye degradation and the only difference is the dye solution was replaced by 5×10^{-3} M terephthalic acid aqueous solution containing 0.01 M NaOH. After reaction for every 30 min, the sample solution was centrifuged and analyzed by the PL spectrum.

(c) Determination of H_2O_2 ^{S6}

10 mg of catalyst was added into 40 mL of DI H_2O and stirred in the dark for 30 min to achieve the adsorption-desorption equilibrium. Afterward, the reaction was irradiated under visible ($\lambda > 420$ nm) light for 25 min. The sample was then collected and centrifuged (12000 rpm) for every 5 min to obtain the supernatant solution, in which 50 μL of DPD was added and shaken manually, followed by adding 50 μL of POD. After 2 min, the final solution was analyzed by UV-absorption spectra to determine whether the two peaks at 510 and 551 nm appear in the UV-vis region ranging from 450 to 600 nm.

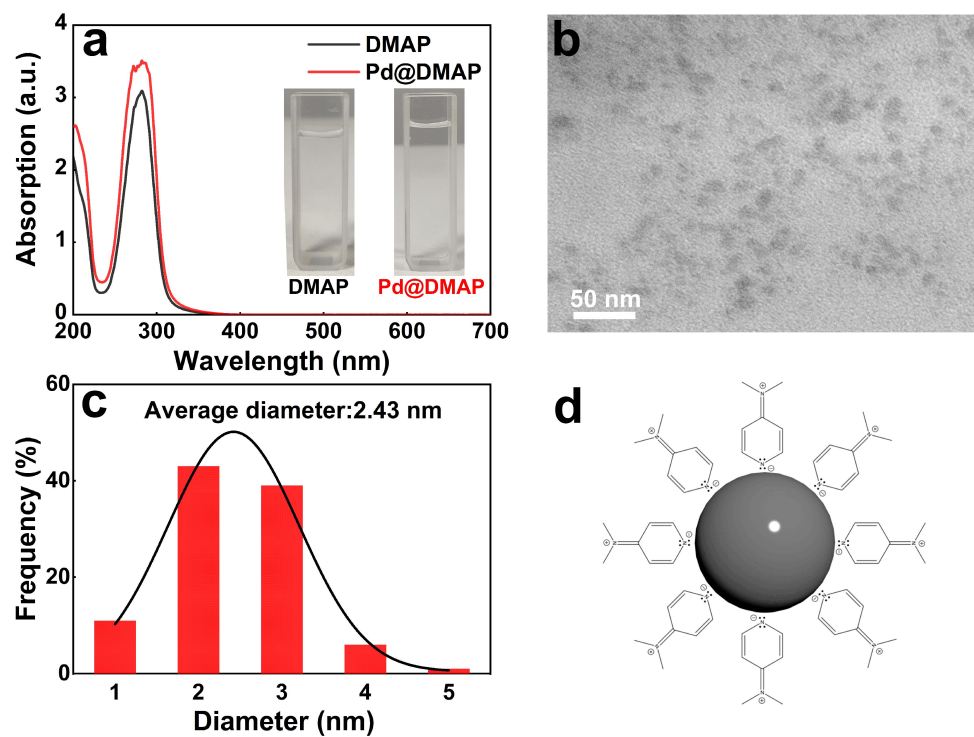


Fig. S1. (a) UV-vis absorption spectra of DMAP and Pd@DMAP NCs colloidal solutions, (b) TEM image of Pd@DMAP NCs with (c) size distribution histogram and (d) molecule structure of DMAP ligand capped on the Pd surface.

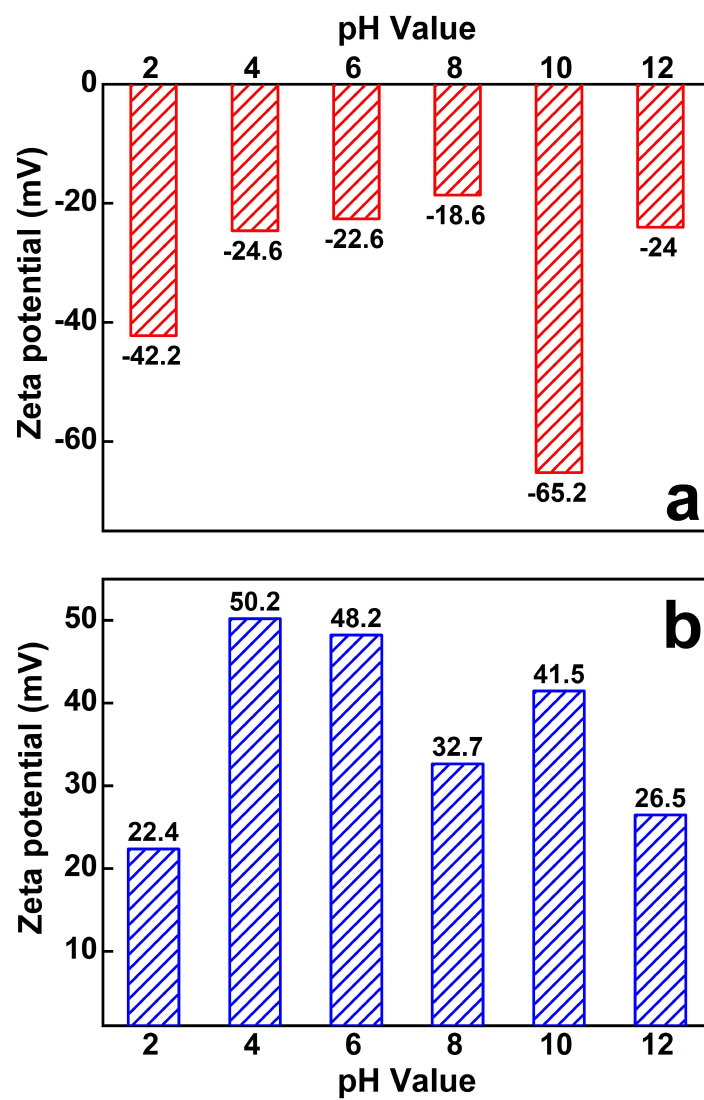


Fig. S2. Zeta potentials of (a) WO₃ NRs and (b) Pd@DMAP NCs.

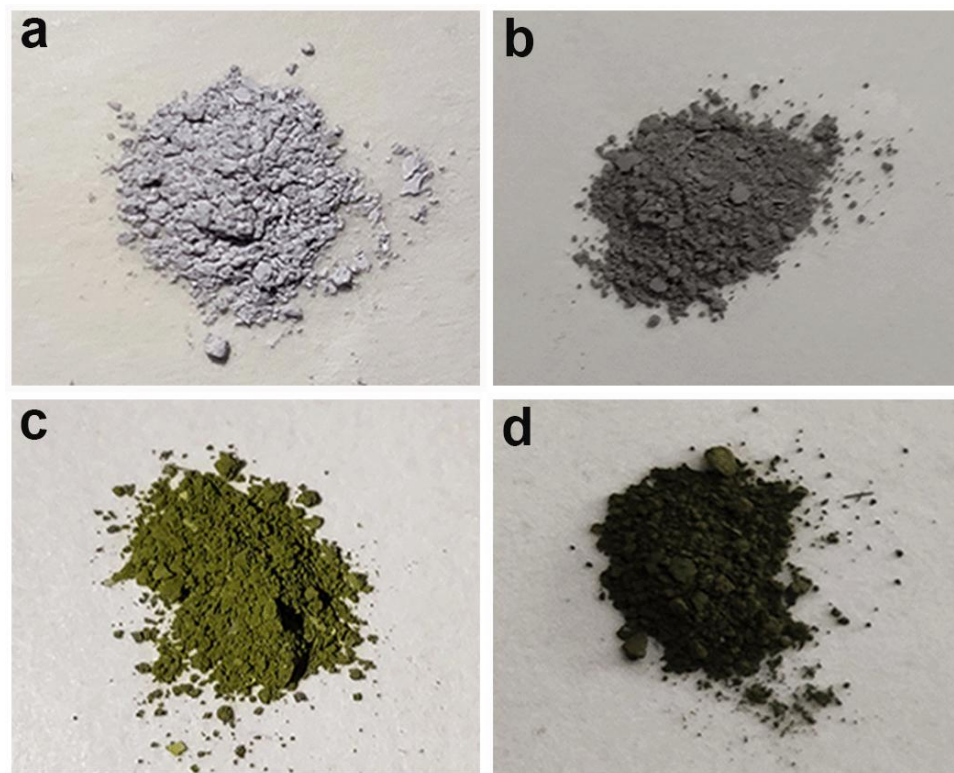


Fig. S3. Photographs of (a) WO_3 NRs, (b) WO_3 NRs@Pd, (c) WO_3 NRs@CdS and (d) WO_3 NRs@Pd@CdS.

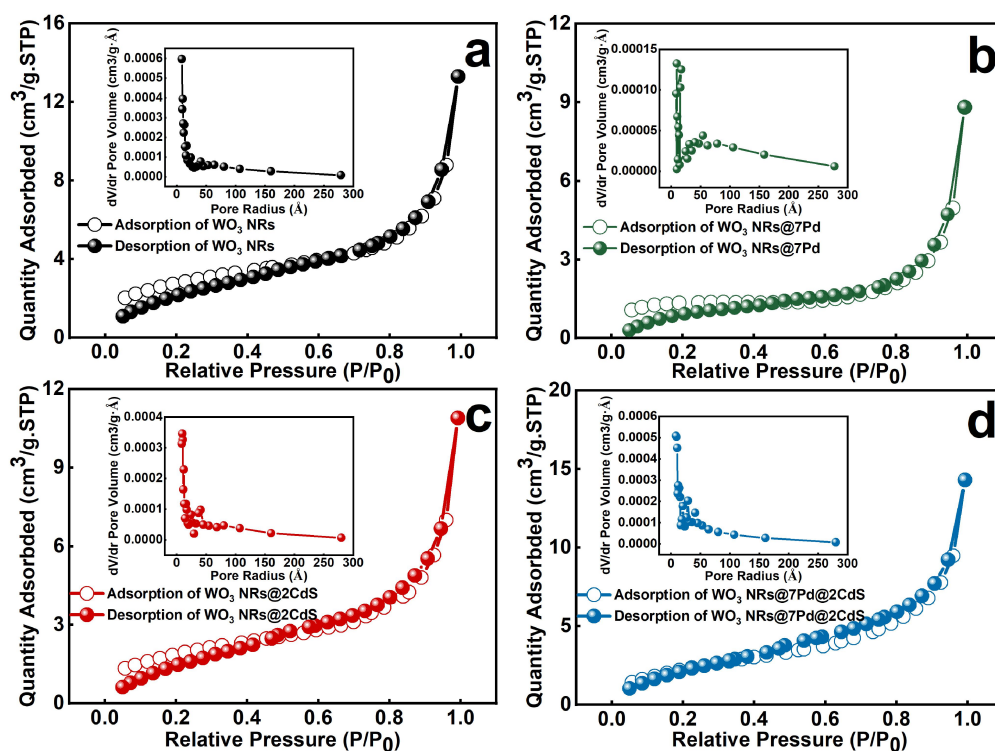


Fig. S4. Nitrogen adsorption-desorption isotherms of (a) WO₃ NRs, (b) WO₃ NRs@Pd, (c) WO₃ NRs@CdS and (d) WO₃ NRs@Pd@CdS heterostructure with pore size distribution plots in the inset.

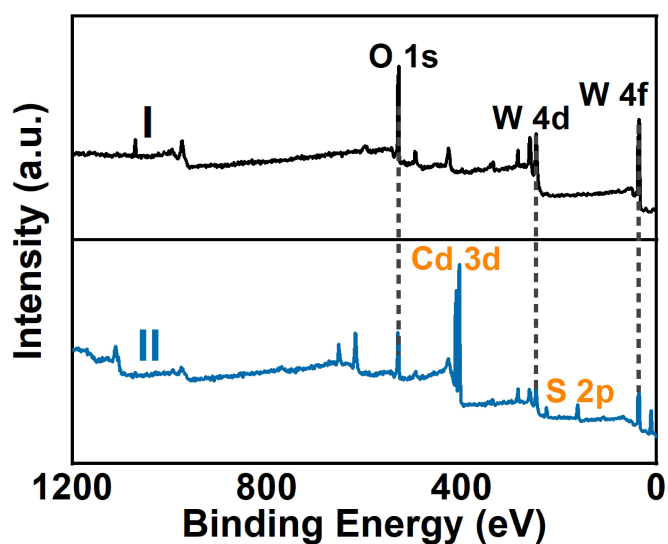


Fig. S5. Survey spectra of (I) WO₃ NRs and (II) WO₃ NRs@Pd@CdS.

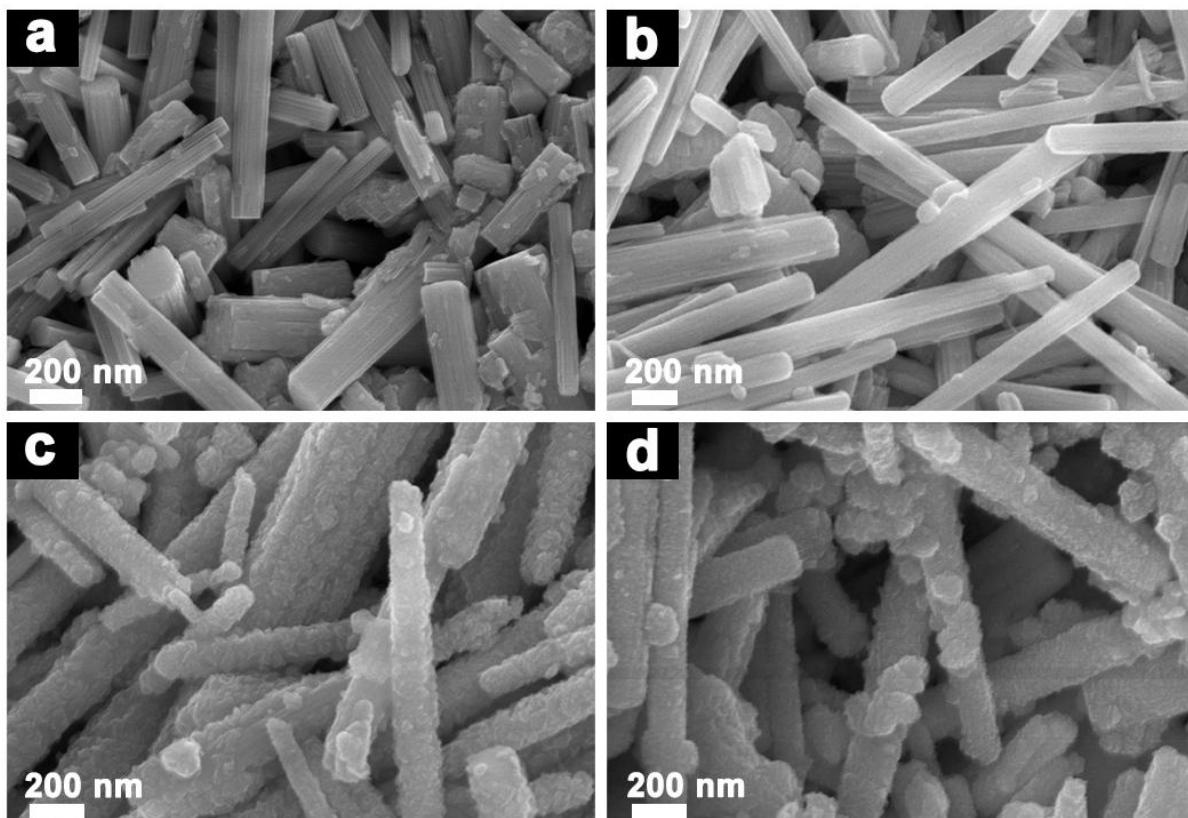


Fig. S6. FESEM images of (a) WO_3 NRs, (b) WO_3 NRs@Pd, (c) WO_3 NRs@CdS and (d) WO_3 NRs@Pd@CdS heterostructure.

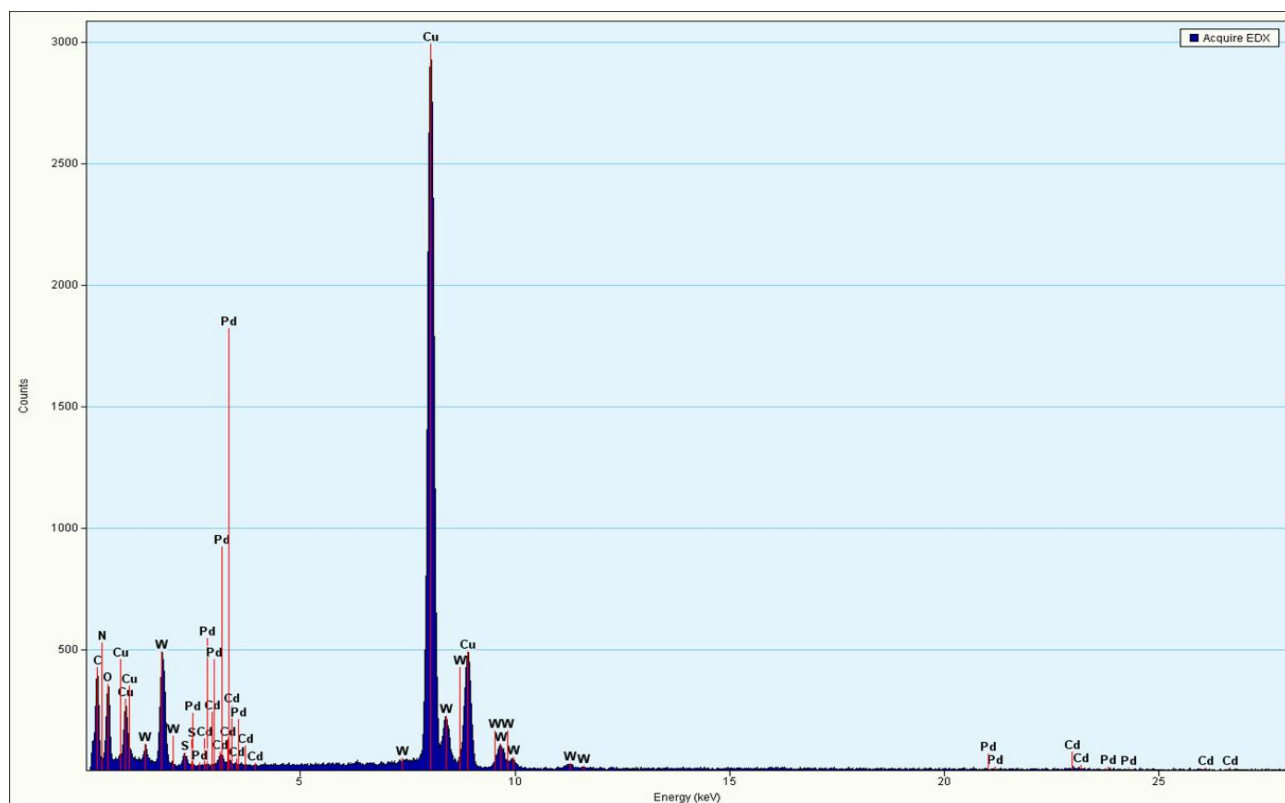


Fig. S7. EDS result of WO₃ NRs@Pd@CdS.

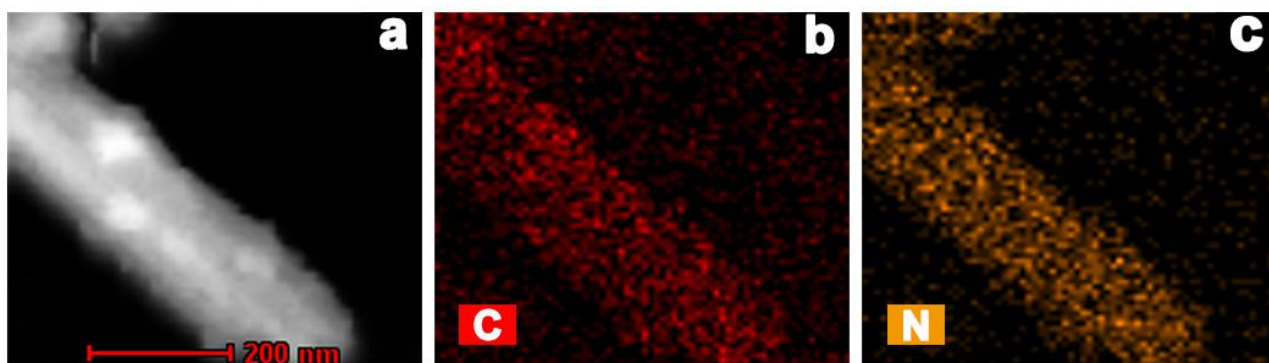


Fig. S8. (a) Elemental mapping results of (b) C and (c) N signals for WO_3 NRs@Pd@CdS.

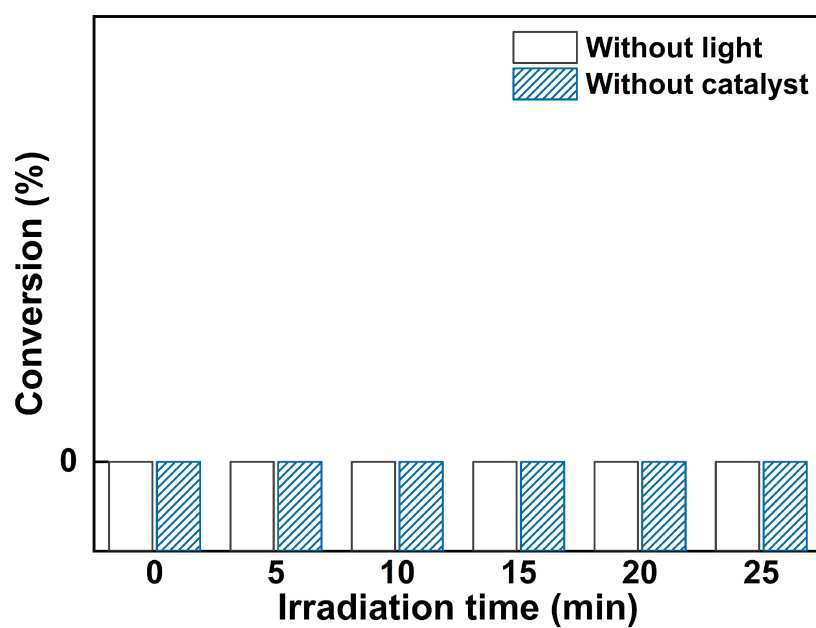


Fig. S9. Blank experiments for photoreduction of 4-NA without light irradiation or catalyst.

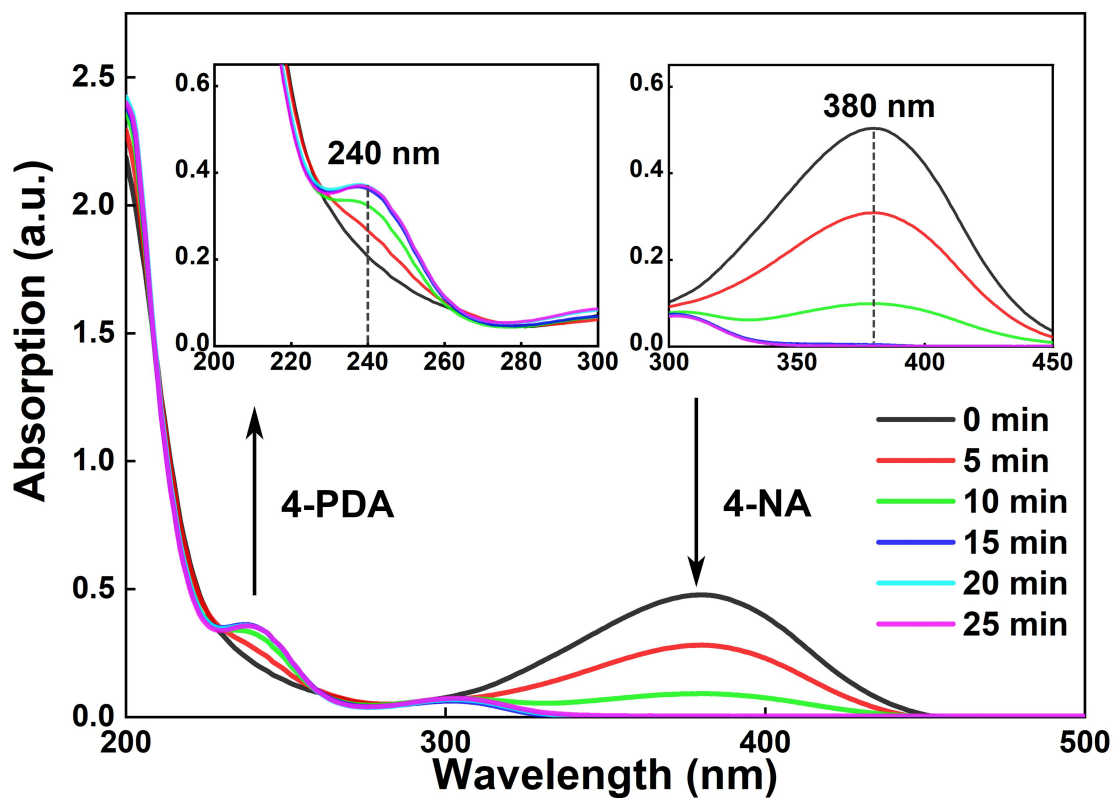


Fig. S10. UV-vis absorption spectra of 4-NA probed after designated irradiation time (25 min) when it was photoreduced in the presence of WO_3 NRs@9Pd@2CdS under visible light irradiation ($\lambda > 420$ nm) with the addition of ammonium formate as hole quencher and N_2 purge under ambient conditions.

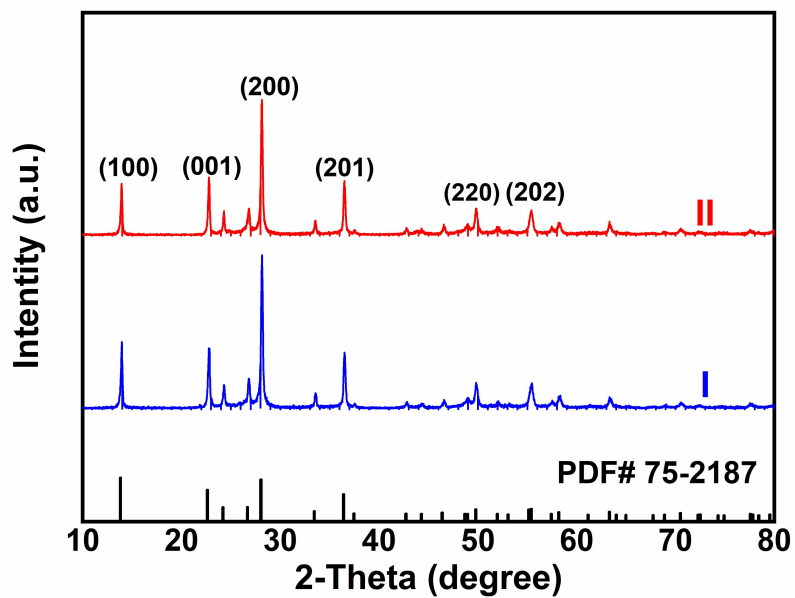


Fig. S11. XRD pattern of WO₃ NRs@7Pd@2CdS (I) before and (II) after cyclic reactions.

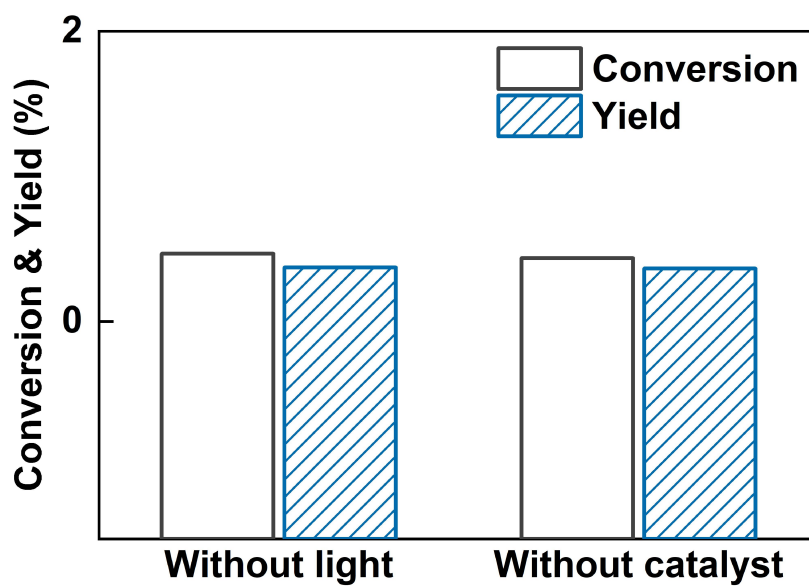


Fig. S12. Blank experiments for photocatalytic selective oxidation of benzyl alcohol without light irradiation or catalyst.

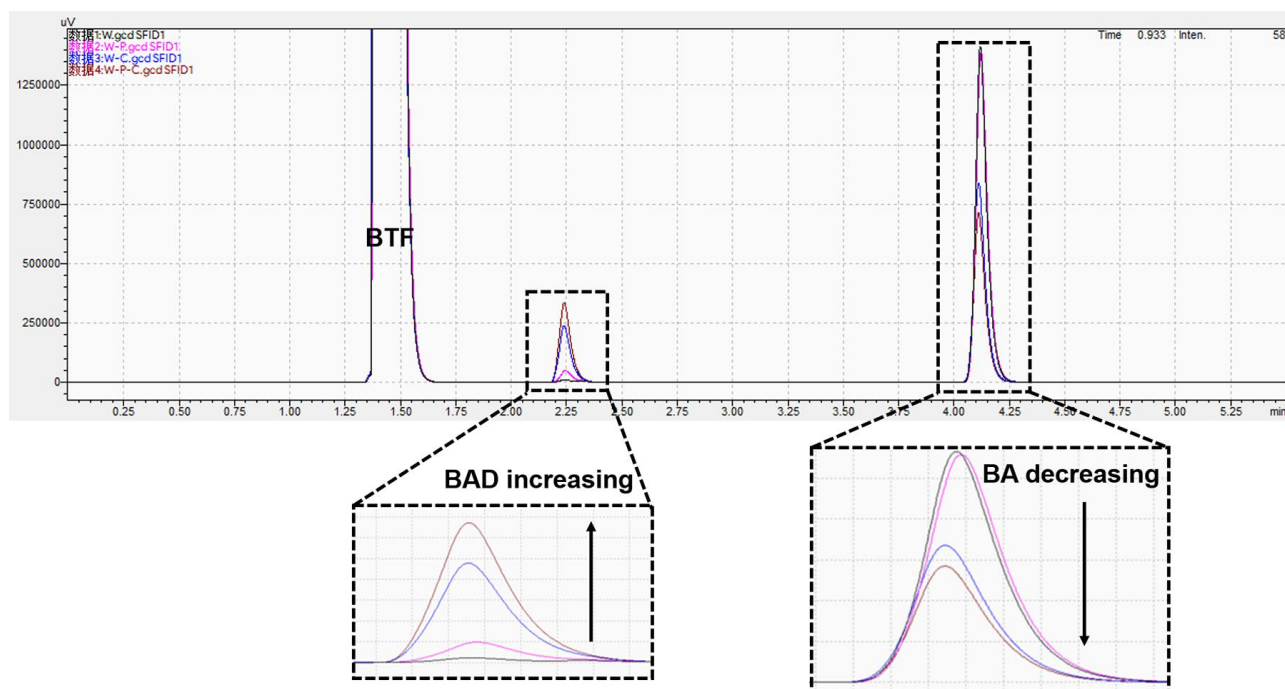


Fig. S13. GC spectra illustrating the photocatalytic selective oxidation of BA to BAD over WO_3 NRs (W -black line), WO_3 NRs@7Pd (WP -red line), WO_3 NRs@2CdS (WC -blue line) and WO_3 NRs@7Pd@2CdS (WPC -brown line) under visible light irradiation ($\lambda > 420$ nm). The peaks from left to right correspond to BTF, BAD and BA, respectively.

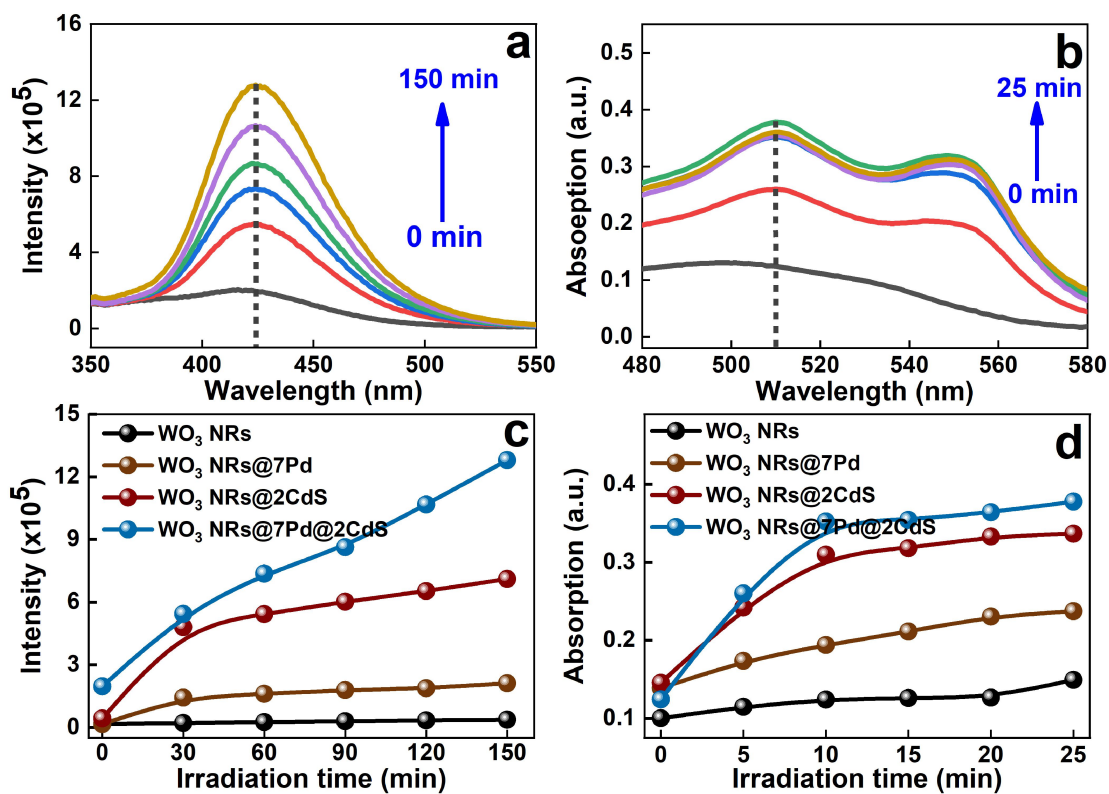


Fig. S14. (a) PL intensity and (b) H_2O_2 production amount of WO_3 NRs@7Pd@2CdS; (c) PL intensity and (d) H_2O_2 production amount comparison among different samples under visible light irradiation ($\lambda > 420$ nm).

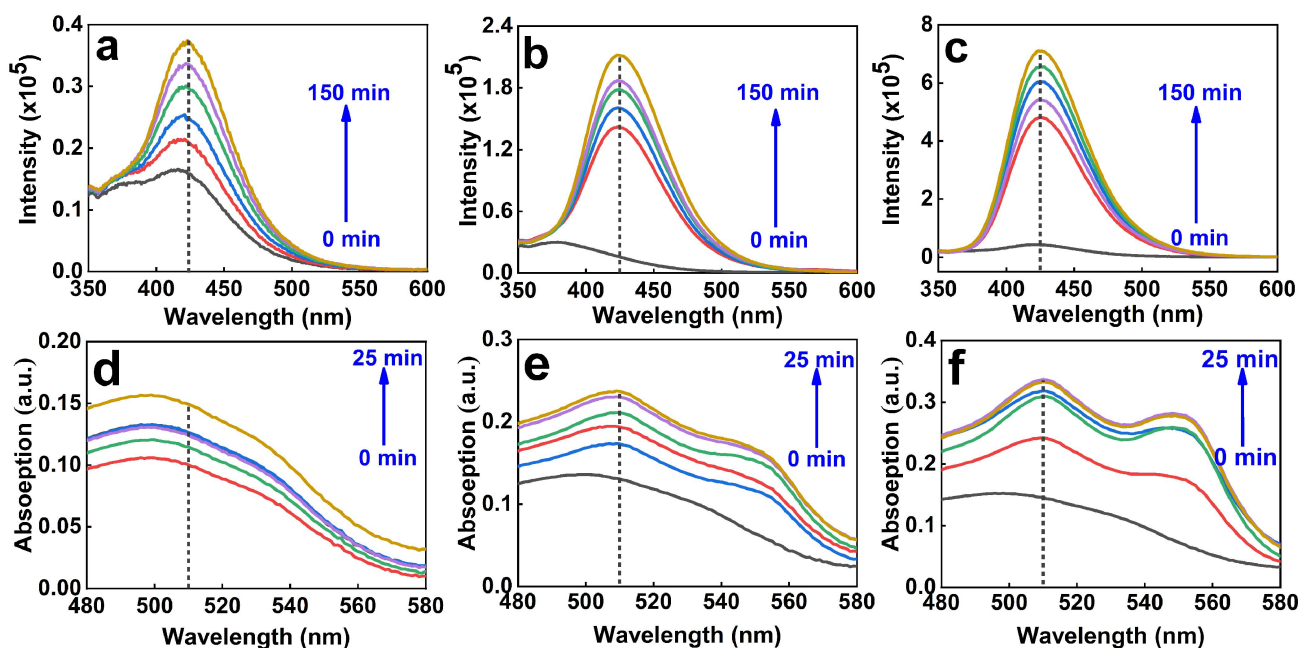


Fig. S15. (a-c) PL spectra and (d-e) H_2O_2 production amount of (a & d) WO_3 NRs, (c & d) WO_3 NRs@7Pd, and (e & f) WO_3 NRs@2CdS.

Note: In-situ production of $\bullet\text{OH}$ radicals in the reaction system was probed by the liquid-phase PL technique.⁴ **Fig. S14a** shows the presence of an apparent peak at 424 nm in the PL spectrum of WO_3 NRs@7Pd@2CdS under the visible light irradiation, implying the formation of $\bullet\text{OH}$ radicals. Moreover, as unveiled in **Fig. S14c** and **Fig. S15 (a-c)**, production amount of $\bullet\text{OH}$ radicals over WO_3 NRs@7Pd@2CdS is larger than WO_3 NRs, WO_3 NRs@7Pd and WO_3 NRs@2CdS under the same conditions. Alternatively, as reflected by **Fig. S14 (b & d)** and **Fig. S15 (d-e)**, WO_3 NRs@7Pd@2CdS still exhibits more enhanced H_2O_2 peak intensity than WO_3 NRs, WO_3 NRs@7Pd and WO_3 NRs@2CdS counterparts under visible light irradiation according to the DPD-POD method.⁶

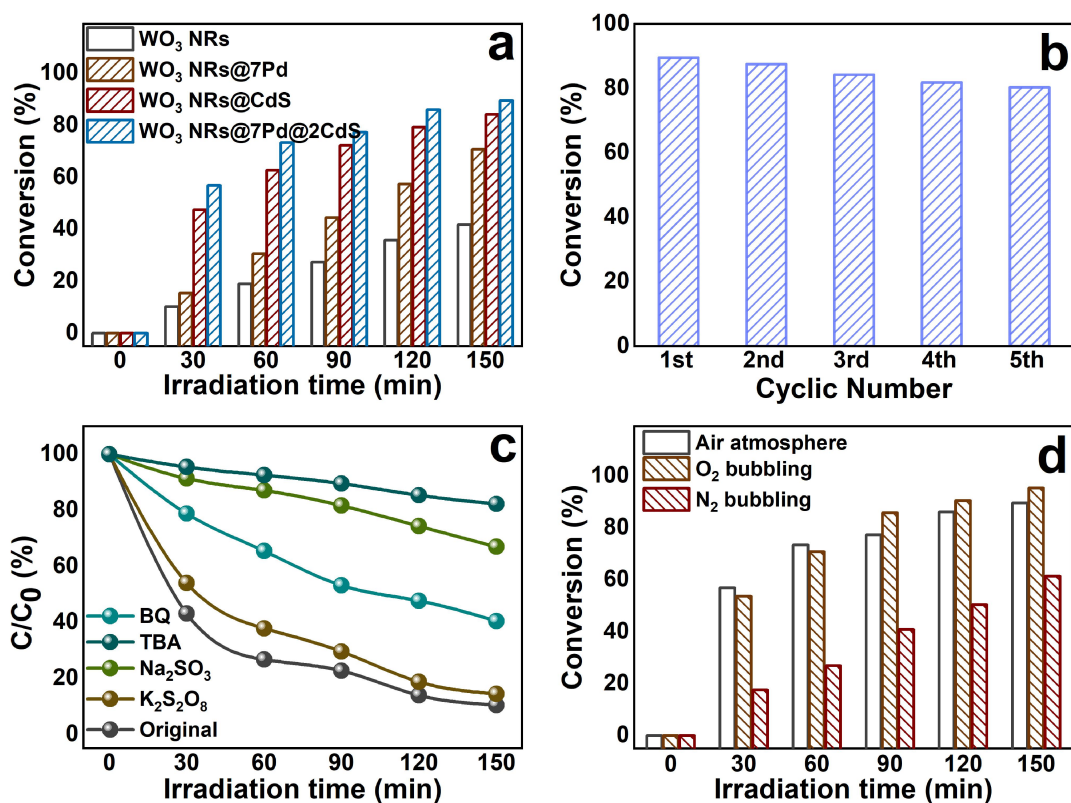


Fig. S16. (a) Photoactivities of WO₃ NRs@7Pd@2CdS toward mineralization of RhB under visible light irradiation ($\lambda > 420$ nm), (b) cyclic reactions of WO₃ NRs@7Pd@2CdS and (c) photoactivity of WO₃ NRs@7Pd@2CdS by adding Na₂SO₃, K₂S₂O₈, BQ and TBA in the reaction system as scavengers for quenching hole (h^+), electrons (e^-), superoxide radicals ($\bullet O_2^-$) and hydroxyl radicals ($\bullet OH$), respectively. (d) Photoactivities of WO₃ NRs@7Pd@2CdS with O₂ and N₂ bubbling under visible light ($\lambda > 420$ nm) irradiation.

Note: As exhibited in **Fig. S16a**, WO₃ NRs@7Pd@2CdS exhibited the most enhanced photo-oxidation performances relative to single and binary counterparts toward RhB degradation under visible light irradiation. The improved photoactivity of WO₃ NRs@7Pd@2CdS arises from the pivotal role of Pd NCs as efficient interfacial electron transfer mediator to accelerate charge transfer rate and the thin CdS layer benefits the construction of Z-scheme charge transport channel. As displayed in **Fig. S16b**, WO₃ NRs@7Pd@2CdS demonstrates good photostability with negligible decay in photoactivity even after five cyclic reactions. **Fig. S16c** shows that photoactivity of WO₃ NRs@7Pd@2CdS were substantially decreased when Na₂SO₃, K₂S₂O₈, BQ and TBA scavengers were added in the reaction system, suggesting holes (h^+), electrons (e^-), $\bullet OH$ radicals and $\bullet O_2^-$ radicals all contribute to the considerably improved photoactivity of WO₃ NRs@7Pd@2CdS toward mineralization of RhB, which is similar to the results of photocatalytic selective oxidation of aromatic alcohols. **Fig. S16d** manifests photoactivity of WO₃ NRs@7Pd@2CdS with O₂ bubbling is improved, indicating dissolved oxygen is beneficial for boosting the photo-oxidation performances owing to producing more oxygen-containing active species such as hydrogen peroxide (H₂O₂), superoxide, and hydroxyl radicals in the reaction system, while N₂ bubbling is detrimental to the photoactivity enhancement.

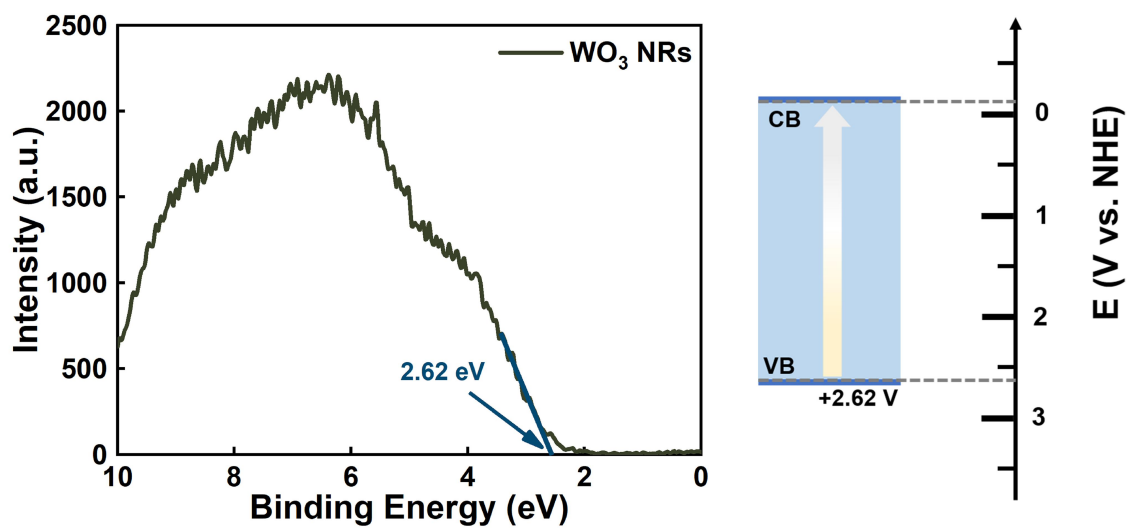


Fig. S17. VB XPS spectrum of WO₃ NRs.

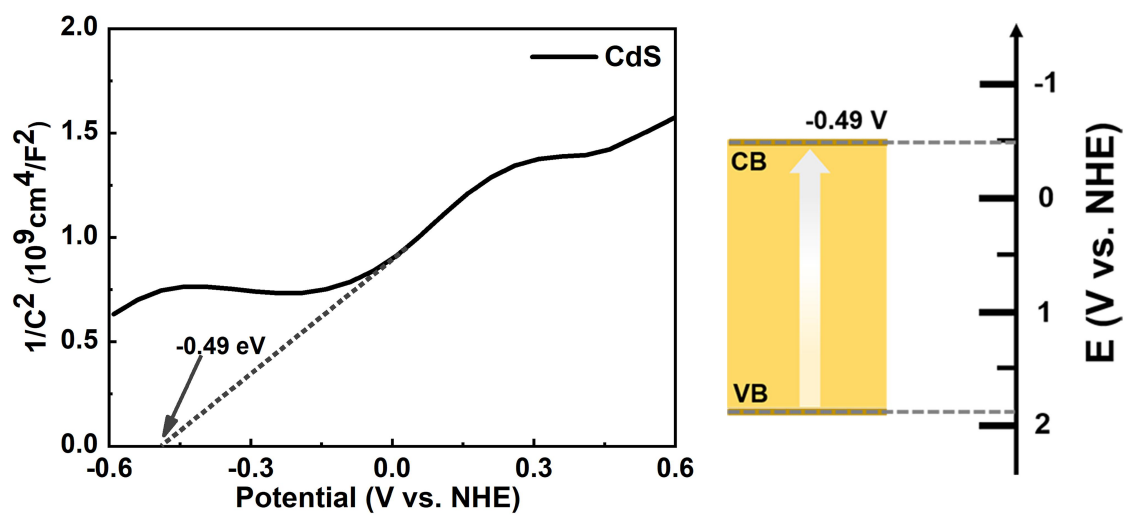


Fig. S18. Mott-Schottky result of CdS.

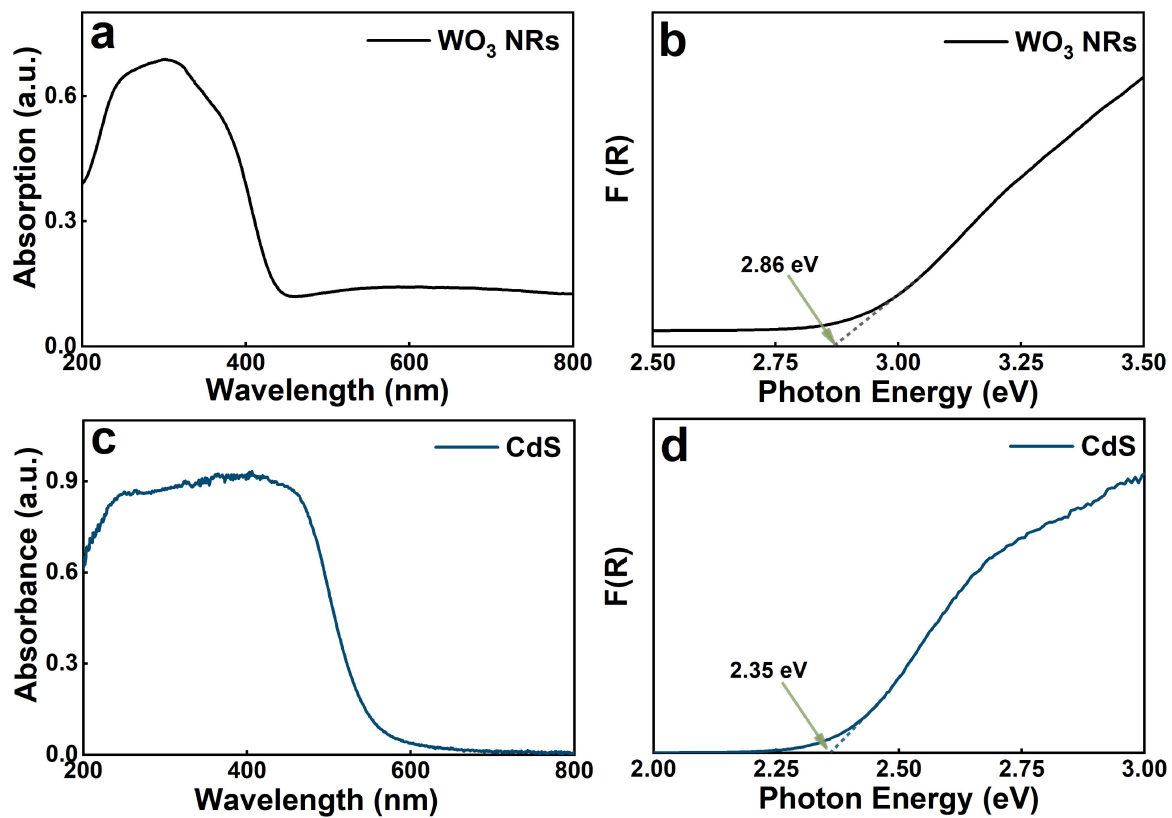


Fig. S19. DRS results of (a & b) WO₃ NRs and (c & d) CdS with transformed plots based on the Kubelka-Munk function vs. energy of light.

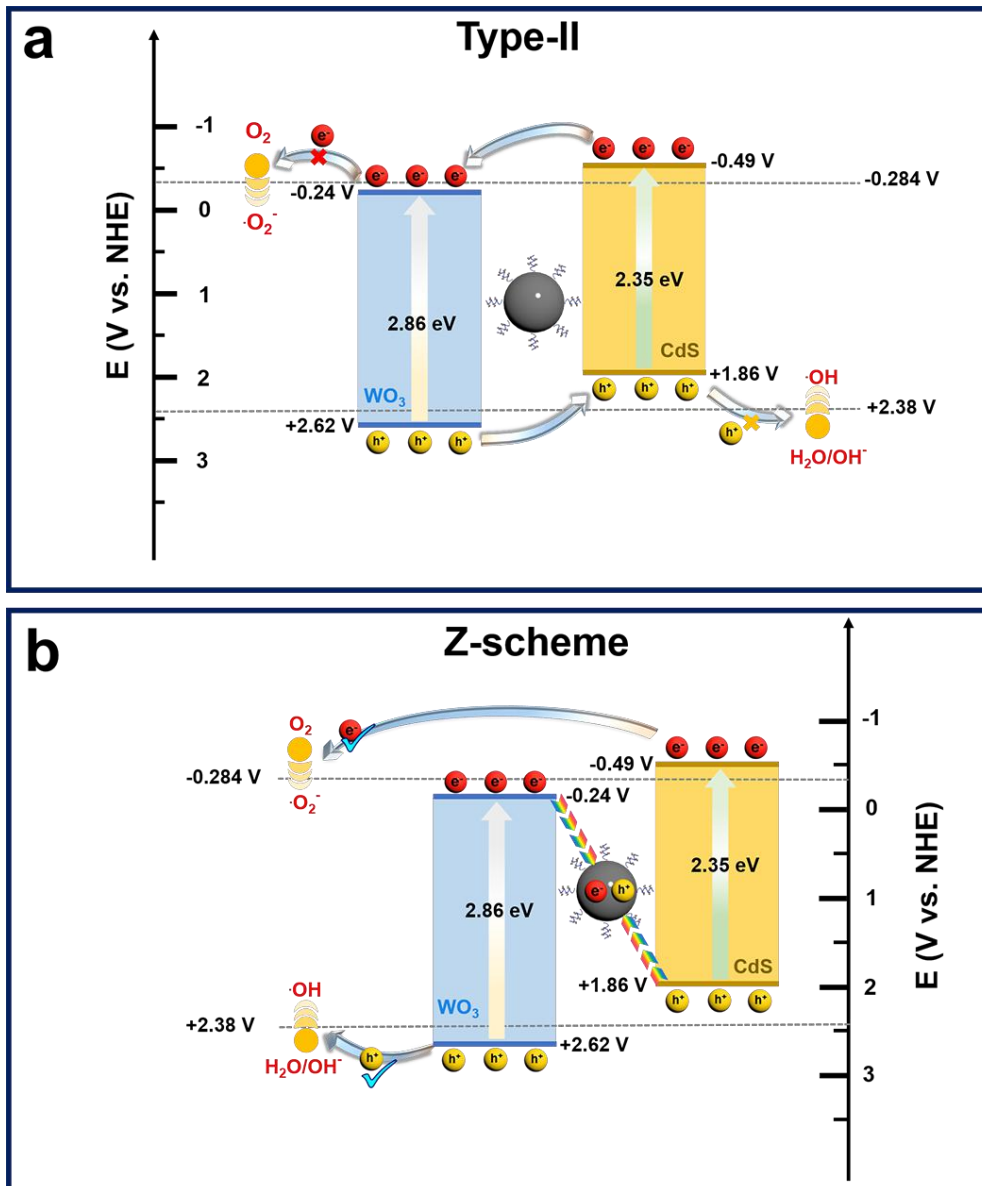


Fig. S20. (a) Type-II and (b) Z-scheme charge transfer mechanisms.

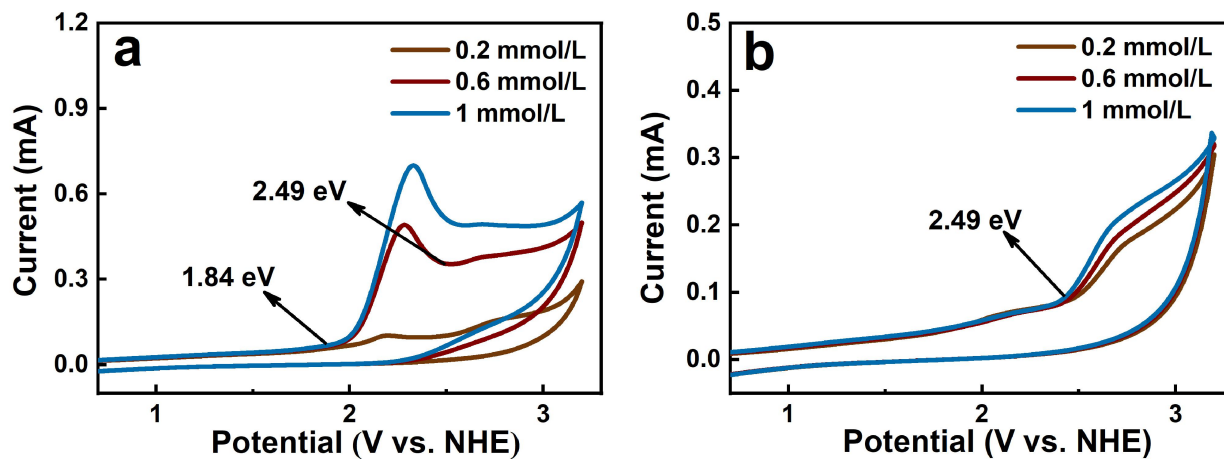


Fig. S21. CV curves of (a) BA and (b) BAD with different concentration (0.2, 0.6, 1 mmol/L).

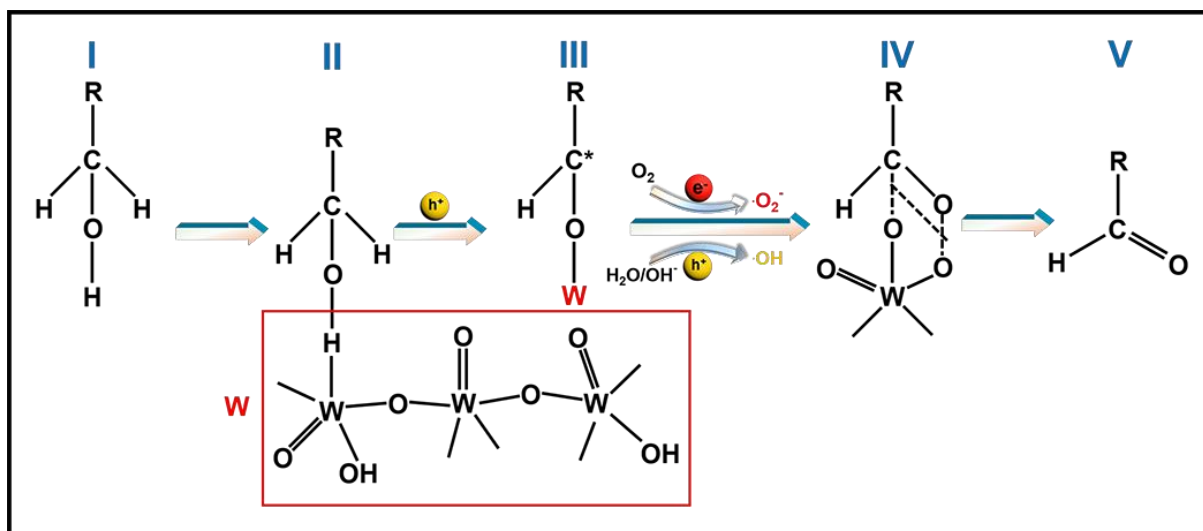


Fig. S22. Mechanism diagram of the selective photocatalytic oxidation of BA to BAD.

Table S1. Peak position with corresponding functional groups.

Peak position (cm ⁻¹)	WO ₃ NRs	WO ₃ NRs@Pd@CdS
3446.91	O-H stretching vibration	O-H stretching vibration ^{S7}
2924.31/2834.52	N.D.	C-H stretching vibration ^{S8}
1612.84	N.D.	N-H deformation vibration ^{S9-10}
1619.24	O-H deformation vibration	O-H deformation vibration ^{S11-12}
824.51	O-W stretching vibrations	O-W stretching vibrations ^{S1}

N.D.: Not Detected

Table S2. Specific surface area, pore volume and pore size of WO₃ NRs, WO₃ NRs@Pd, WO₃ NRs@CdS and WO₃ NRs@Pd@CdS heterostructure.

Samples	S _{BET} (m ² /g) ^a	Total pore volume (cm ³ /g) ^b	Average pore size (Å) ^c
WO ₃ NRs	9.5431	0.011985	49.8456
WO ₃ NRs@Pd	4.0873	0.006479	60.0112
WO ₃ NRs@CdS	6.5592	0.009614	56.0657
WO ₃ NRs@Pd@CdS	8.7190	0.013131	60.2481

a. BET surface area is calculated from the linear part of BET plots.

b. Single point total pore volume of the pores at P/P₀ = 0.99.

c. Adsorption average pore width (4V/A by BET).

Table S3. Chemical bond species vs. B.E. for different samples.

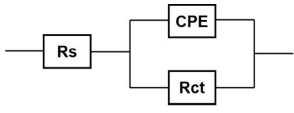
Elements	WO ₃ NRs	WO ₃ NRs@Pd@CdS	Chemical Bond Species
W 4f _{7/2}	35.50	35.55	(W ⁶⁺)
W 4f _{5/2}	37.70	37.65	(W ⁶⁺) ^{S1, S13}
O 1s _{1/2}	530.45	530.5	(W-O) ^{S14}
O 1s _{1/2}	531.65	532.05	(H-O) ^{S14}
Cd 3d _{5/2}	N.D.	405.2	(Cd ²⁺)
Cd 3d _{3/2}	N.D.	411.95	(Cd ²⁺) ^{S15-16}
S 3d _{3/2}	N.D.	161.45	(S ²⁻)
S 3d _{1/2}	N.D.	162.7	(S ²⁻) ^{S9, S17}
Pd 3d _{5/2}	N.D.	336.5	(Pd ⁰)
Pd 3d _{3/2}	N.D.	341.9	(Pd ⁰) ^{S18-19}
N 1s	N.D.	N.D.	(N-H) ^{S1}

N.D.: Not Detected

Table S4. Kinetic rate constants of different samples.

Sample	Kinetic rate constant (min⁻¹)
WO ₃ NRs	0.002
WO ₃ NRs@11Pd	0.00433
WO ₃ NRs@11Pd@1CdS	0.03576
WO ₃ NRs@11Pd@2CdS	0.21003
WO ₃ NRs@11Pd@3CdS	0.20567
WO ₃ NRs@11Pd@4CdS	0.16464
WO ₃ NRs@11Pd@5CdS	0.00543
CdS	0.01486
WO ₃ NRs@2CdS	0.07228
WO ₃ NRs@3Pd@2CdS	0.03997
WO ₃ NRs@5Pd@2CdS	0.16769
WO ₃ NRs@7Pd@2CdS	0.28715
WO ₃ NRs@9Pd@2CdS	0.24484
WO ₃ NRs@11Pd@2CdS	0.21003

Table S5. Fitted EIS results of different photoanodes based on the equivalent circuit under visible ($\lambda > 420$ nm) light irradiation.

<i>Photoanodes</i>	<i>R_s/ohm</i>	<i>R_{ct}/ohm</i>	<i>CPE/(F·cm⁻²)</i>	<i>Equivalent Circuit</i>
WO ₃ NRs	13.64	17140	7.905E-5	
WO ₃ NRs@7Pd	13.96	9872	7.346E-5	
WO ₃ NRs@2CdS	21.43	7857	8.989E-5	
WO ₃ NRs@7Pd@2CdS	15.99	6529	7.459E-5	

References

- S1. B. Weng, J. Wu, N. Zhang and Y. J. Xu, *Langmuir*, 2014, **30**, 5574-5584.
- S2. D. I. Gittins and F. Caruso, *Angew. Chem. Int. Edit.*, 2001, **40**, 3001-3004.
- S3. N. Zhang, S. Xie, B. Weng and Y.-J. Xu, *J. Mater. Chem. A*, 2016, **4**, 18804-18814.
- S4. X. Lin, Z.-Q. Wei, T. Li, M.-H. Huang, S. Xu, Y. He, G. Xiao and F.-X. Xiao, *Inorg. Chem.*, 2020, **59**, 1364-1375.
- S5. H.-J. Lin, T. Li, M.-H. Huang, X.-C. Dai, Y.-B. Li and F.-X. Xiao, *J. Phys. Chem. C*, 2019, **123**, 28066-28080.
- S6. H. Bader, V. Sturzenegger and J. Hoigné, *Water Res.*, 1988, **22**, 1109-1115.
- S7. Z.-Q. Wei, X.-C. Dai, S. Hou, Y.-B. Li, M.-H. Huang, T. Li, S. Xu and F.-X. Xiao, *J. Mater. Chem. A*, 2020, **8**, 177-189.
- S8. M.-H. Huang, X.-C. Dai, T. Li, Y.-B. Li, Y. He, G. Xiao and F.-X. Xiao, *J. Phys. Chem. C*, 2019, **123**, 9721-9734.
- S9. T. Li, Y.-B. Li, X.-C. Dai, M.-H. Huang, Y. He, G. Xiao and F.-X. Xiao, *J. Phys. Chem. C*, 2019, **123**, 4701-4714.
- S10. Y. Su, Z. Han, L. Zhang, W. Wang, M. Duan, X. Li, Y. Zheng, Y. Wang and X. Lei, *Appl. Catal. B*, 2017, **217**, 108-114.
- S11. M. Seifollahi Bazarjani, M. Hojamberdiev, K. Morita, G. Zhu, G. Cherkashinin, C. Fasel, T. Herrmann, H. Breitzke, A. Gurlo and R. Riedel, *J. Am. Chem. Soc.*, 2013, **135**, 4467-4475.
- S12. G. Xi, J. Ye, Q. Ma, N. Su, H. Bai and C. Wang, *J. Am. Chem. Soc.*, 2012, **134**, 6508-6511.
- S13. Z.-Y. Liang, J.-X. Wei, X. Wang, Y. Yu and F.-X. Xiao, *J. Mater. Chem. A*, 2017, **5**, 15601-15612.
- S14. F. Xu, Y. Yao, D. Bai, R. Xu, J. Mei, D. Wu, Z. Gao and K. Jiang, *RSC Adv.*, 2015, **5**, 60339-60344.
- S15. Y.-B. Li, T. Li, X.-C. Dai, M.-H. Huang, Y. He, G. Xiao and F.-X. Xiao, *J. Mater. Chem. A*, 2019, **7**, 8938-8951.
- S16. S. Xu, M.-H. Huang, T. Li, Z.-Q. Wei, X. Lin, X.-C. Dai, S. Hou, X.-Y. Fu and F.-X. Xiao, *J. Mater. Chem. A*, 2020, **8**, 8360-8375.
- S17. X.-Y. Fu, Y.-B. Li, M.-H. Huang, T. Li, X.-C. Dai, S. Hou, Z.-Q. Wei and F.-X. Xiao, *Inorg. Chem.*, 2020, **59**, 2562-2574.
- S18. K. R. Priolkar, P. Bera, P. R. Sarode, M. S. Hegde, S. Emura, R. Kumashiro and N. P. Lalla, *Chem. Mater.*, 2002, **14**, 2120-2128.
- S19. R. A. Campbell, J. Rodriguez and D. W. Goodman, *Surf. Sci.*, 1990, **240**, 71-80.